JOURNAL OF MATERIALS SCIENCE **37** (2002) 2279–2292

Fatigue crack growth of DSX40M alloy at ambient and elevated temperatures

M. AHMAD
Radiation Damage Group, Nuclear Physics Division, Pakistan Institute of Nuclear Science and Technology, P.O. Nilore Islamabad, Pakistan

Y. B. XU, GE. YAO, Z. Q. HU
State Key Laboratory for Fatigue and Fracture of Materials, Institute of Metal Research, Academia Sinica, Schenyang 110015, People's Republic of China

Fatigue crack propagation behaviour of compact tension specimens of DSX40M alloy has been investigated in air at room temperature and at 850°C. The results indicate that the crystallographic cracking occurs on two or more planes simultaneously at room temperature. Slip bands are observed along the crack. Crack growth is affected by the temperature. The fatigue crack growth is higher at elevated temperature than room temperature. Microcracks start at the precipitates/eutectic and join the fatal crack. The number of planes intersecting each other determines the different microscopic features on the cleavage fracture surface. Dislocation structure in the plastic zone underneath the crack propagation at room temperature and at 850°C has been investigated by transmission electron microscopy. Dislocation pile up starts at lower ΔK and dislocations are moving in a planar slip and few of the dislocations form network in the final broken area at room temperature. At 850°C the dislocations are piling up at lower ΔK and dislocations are dispersing and forming network at higher ΔK. The complete network formation was observed in the final broken area at 850°C. The dislocation density is very much higher at 850°C compared to that at room temperature.

1. Introduction

Co-base superalloys are used in industrial gas turbine as nozzle guide vane material due to their good hot corrosion resistance under sulfurizing environment. Nozzle guide vanes direct the hot gases onto the rotating stage of the turbine at the most favourable angle of incidence. The shape of the nozzle guide vanes does not allow the same degree of cooling in all the area of the component so that uneven heating and cooling is the cause of thermal fatigue cracking in particular at both leading and trailing edges because in steady state operation leading edges experience the highest temperature as well as the highest gas bending stress [1], particularly in the case of rapid acceleration of the jet fighter, a sudden rise of inlet temperature of jet engine occurs.

In general, crack nucleates at persistent slip bands or usually at the intersection of grain boundaries with the free surface in pure metals and propagates usually in two stages [2]. In most of the metallic materials fatigue cracks initiate along crystallographic slip planes and then propagate to a direction approximately normal to the load axis. The former cracking mode is called stage I and the latter is called stage II mode due to its non crystallographic behaviour. The crystallographic stage I fatigue is widely observed in some high strength structural alloys such as Al-base [3], Ni-base [4, 5] and brass [6]. The fatigue crack path in these materials occur along the planes which are subjected to large shear stress and shear strain and this "slip band decohesion" process is usually characterized by a cleavage like brittle fracture. Koss and Chan [7] suggested that the extended stage I crack growth and the associated cleavage like brittle fracture surface appearance is the consequence of the crack-tip plasticity and in particular the inability of coplanar slip to relax the normal stress component of the crack-tip field.

Although limited studies on low cycle fatigue and fatigue crack propagation in cobalt base aligned eutectic alloys have been performed at room temperature, no report has been found on crack growth rate and mechanism of crack propagation under high cycle fatigue on DSX40M alloy. The aim of the present study is to investigate the fatigue crack growth behaviour and mechanism of crack propagation of DSX40M alloy in air at room temperature and at 850°C.

2. Experimental

The chemical composition of the alloy used in the present study is given in Table I. Compact-tension specimens (CT) were fabricated from the sheet using a spark cutting machine according to the ASTM standard [8] and the design of the specimen is shown in Fig. 1. The notch root radius is approximately 140 μm and notch

TABLE I Composition of the DSX40M alloy (wt%)

Cr	Ni	W	Al	Ta	Mo	Ti	C	Zr	B	Co
25	11.0	7.5	0.8	0.25	0.2	0.15	0.45	0.15	0.05	Balance

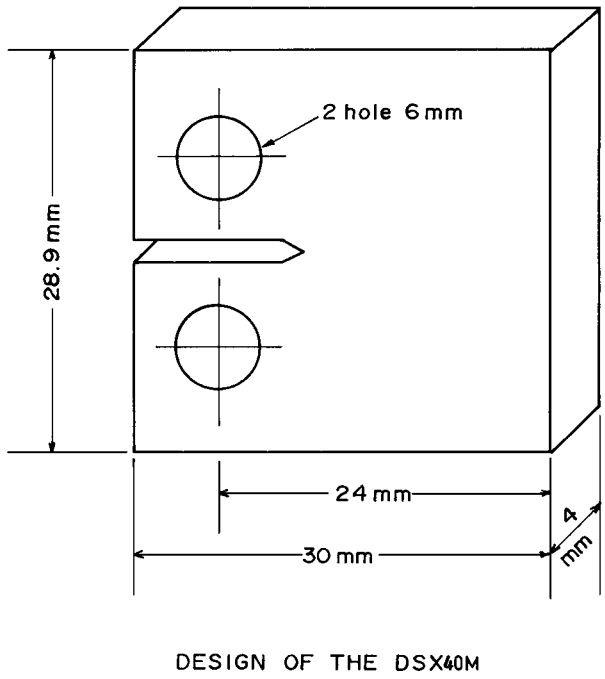

Figure 1 Design of DSX40M alloy compact tension specimen.

length and notch width are about 10 mm and 300 μm respectively. After machining, the samples were polished on 600# and 1000# grade SiC papers and afterward on cloth using diamond paste up to 25 μm to observe the crack propagation. Fatigue tests were conducted with a constant load, stress ratio ($R = P_{\min}/P_{\max}$) is 0.1, and frequency 30 Hz. Schenck servo hydraulic machines having load of 10 KN and 50 KN were used for room temperature and elevated temperature (850°C) respectively.

The crack initiation and propagation was monitored using D.C potential drop apparatus at elevated temperature i.e. 850°C and was measured on both sides of the samples optically using travelling microscope with an accuracy of 0.1 mm at room temperature. Tests at room temperature were interrupted periodically in order to examine the cracking behaviour in scanning electron microscope (SEM). The crack length at elevated temperature was evaluated from the electrical potential according to the formula given in [8, 9].

The threshold intensity ΔK_{th} was measured using load shedding method. The fatigue cracks growth rates (FCGRS) and the intensity factor ΔK on the fracture plane normal to the loading axis was calculated using the seven point polynomial method [10]. The fracture surfaces were investigated using the Stereo-Scan 360 Cambridge Scanning Electron Microscope (SEM) attached with Link AN1000 Energy Dispersive System (EDS). After characterizing the surface in the SEM, a layer of 0.2 mm thick was cut from the sample parallel to fracture surface. The broken samples were cut from the notch area, crack propagation area and sudden broken area to investigate the plastic zone underneath the crack tip. The surfaces were polished on 600 grade SiC paper just to get the flat surface. The cut surface was ground to .05 mm. The samples were electrolytically polished in a solution of 10% perchloric acid in ethanol up to perforation and observed in a transmission electron microscope JEM-FX 2000 II.

3. Results and discussion

3.1. Fatigue crack growth rate

The fatigue crack growth rates of DSX40M at ambient and elevated temperature are given in Fig. 2 (a and b) respectively. In both cases the stress ratio is ($R = P_{\min}/P_{\max} = 0.1$). The threshold intensity factor ΔK_{th} at room temperature was calculated to be 9.98 MPa $m^{1/2}$.

The crack growth rate data in Fig. 2 (a and b) show a considerable scatter for several specimens at room temperature and at elevated temperature. This apparent scatter was not due to the experimental technique but it was due to the crack branching, deflection and roughness induced due to crack closure. The crack growth is higher at 850°C compared to room temperature in the Paris regime region which may be due to higher mobility of dislocation.

On the macroscopic scale, all the specimens failed by dominant crack travelling on either a plane or a combination of planes. However, the dominant crack also showed a significant amount of crack branching and deflection. As demonstrated in Fig. 3a, crack branching and deflection occurred as the crack switched to

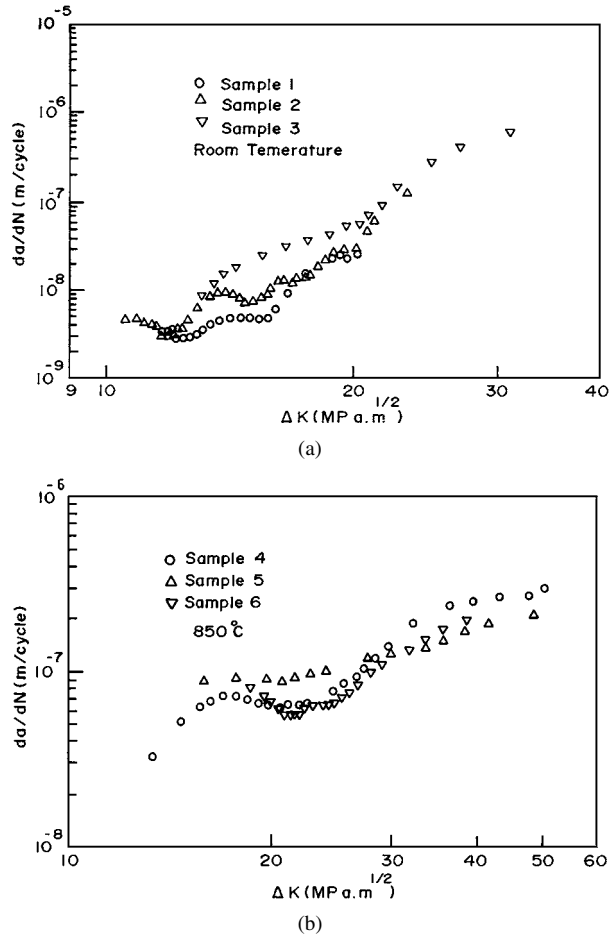

Figure 2 (a) Fatigue crack growth rate as a function of ΔK in air at room temperature. (b) Fatigue crack growth rate as a function of ΔK at 850°C.

propagate along parallel or intersecting slip bands or along the grain boundaries.

3.2. Crack path and fractographic observation at room temperature

It is seen from Fig. 3a microcrack A stopped propagating after it grew over a shorter distance and the other microcrack B could propagate continually and eventually became a macroscopic crack. From Fig. 3a it is clear that once a crack is nucleated and when the stress intensity is low, the crack continues to develop along an active slip plane at about 45° to the loading direction, referred to as stage I. With the increase in crack length, the stress intensity will increase, which promote the slip on the other system and the crack begins to propagate normal to the loading axis, i.e. in stage II by definition. However, as shown in Fig. 3b stage II cracking at a higher magnification, the crack growth is actually characterized by stage I on the microscopic scale. The crack propagates alternately activating on two slip systems. It is clear that two sets of slip traces that are inclined to each other by about 90° are visible near the fatal crack Fig. 3c. It can be explained on the basis of the alternating shear model proposed by Neumann [11] who suggested that when the crack is

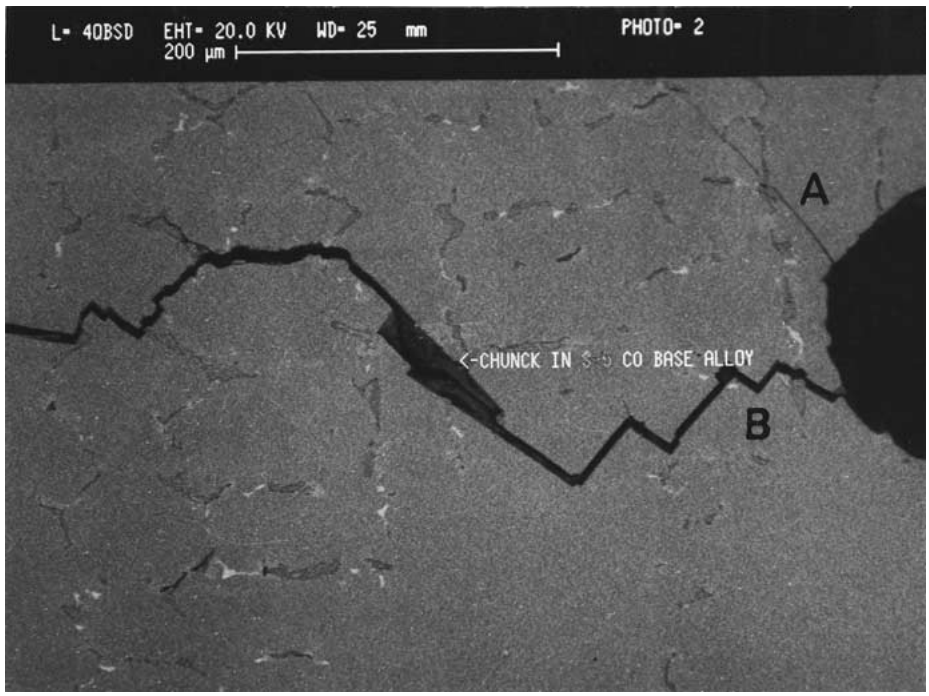

(a)

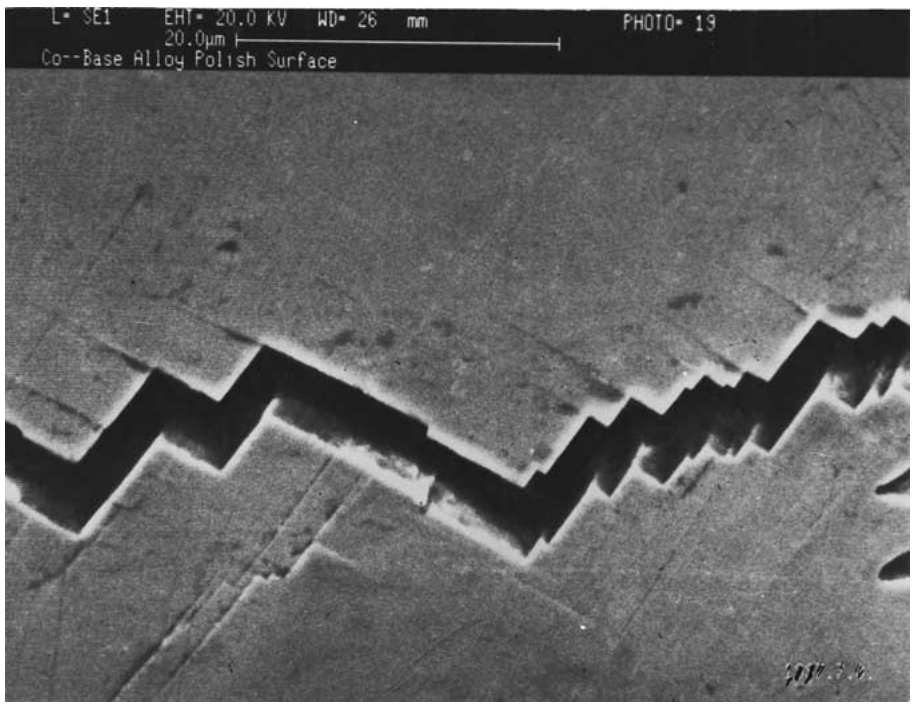

(b)

Figure 3 (a) SEM micrograph showing; (i) the deflection and branching (ii) nucleation of cracks A & B and propagation of the B crack. (b) High magnification micrograh of mode II cracking. (c) SEM micrograph showing the slip band at right angle to each other. (*Continued.*)

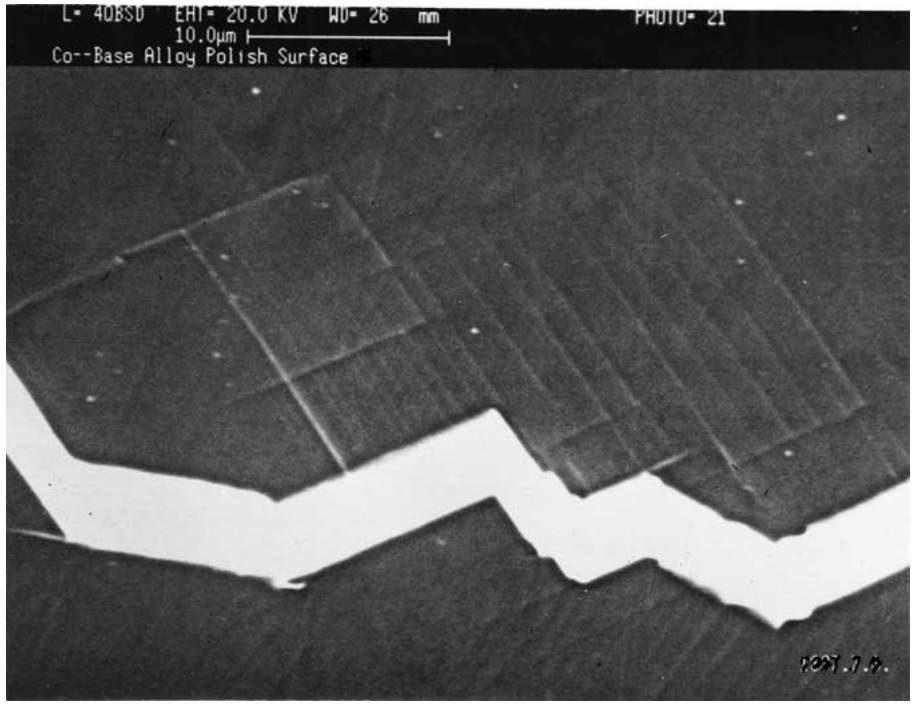

(c)

Figure 3 (*Continued.*)

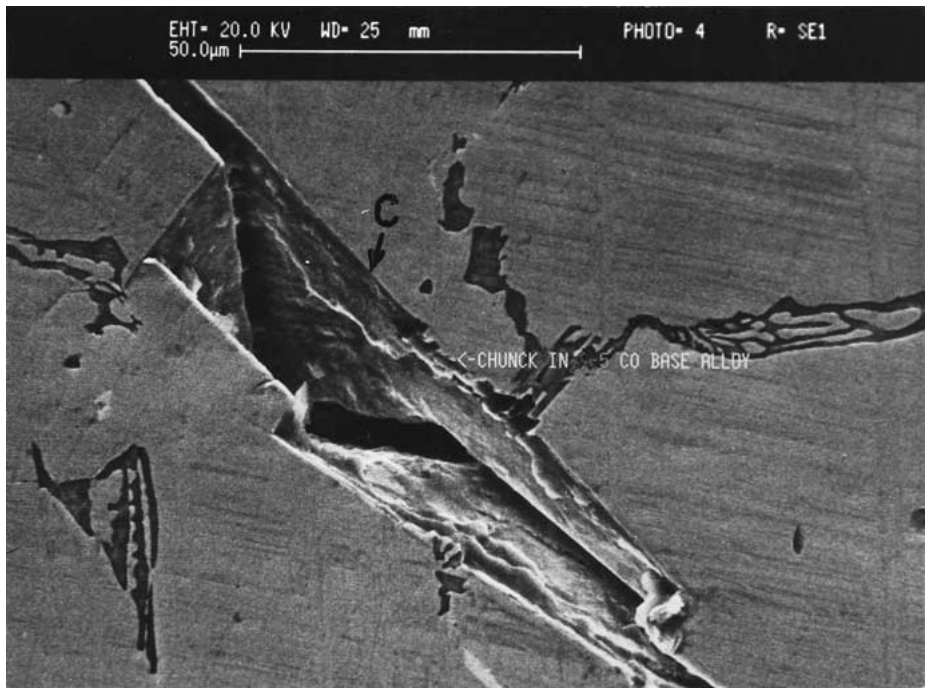

Figure 4 A chunk (indicated by letter 'C') of materials fell out from the specimen surface.

propagating along the primary slip plane, the primary slip system ahead of the crack tip hardens and results in moving the crack tip to a plane where the other system has not been hardened yet. Thus, the crack frequently changes the growth direction from one slip system to another slip system.

In the present case crystallographic cracking along alternative planes occurs indeed. Since cracking occurred/advanced along multiple directions, a chunk of material falling out from the specimen surface was observed, as indicated by letter C in Fig. 4. The size of the chunk is approximately $92 \times 25\,\mu\text{m}^2$. This phenomenon was attributed to the intersection of multiple planes and was also observed in a Mar-M200 single crystal subjected to far field cyclic compression [12] and in $Ni_3Al(Cr,B)$ [13] single crystal fatigue tested at room temperature in air under stress controled condition. It is shown in Fig. 5a, that crack deflected near the grain boundaries and changed its path. It is well documented [14] that for fatigue crack growth in underaged microstructure of precipitation hardened materials, such deflected crack path gives rise to significant amount of roughness-induced crack closure. The black debris was also observed and is shown in Fig. 5b. It is believed that black debris is formed as a result of rubbing of fracture surface during the fatigue cycle. The

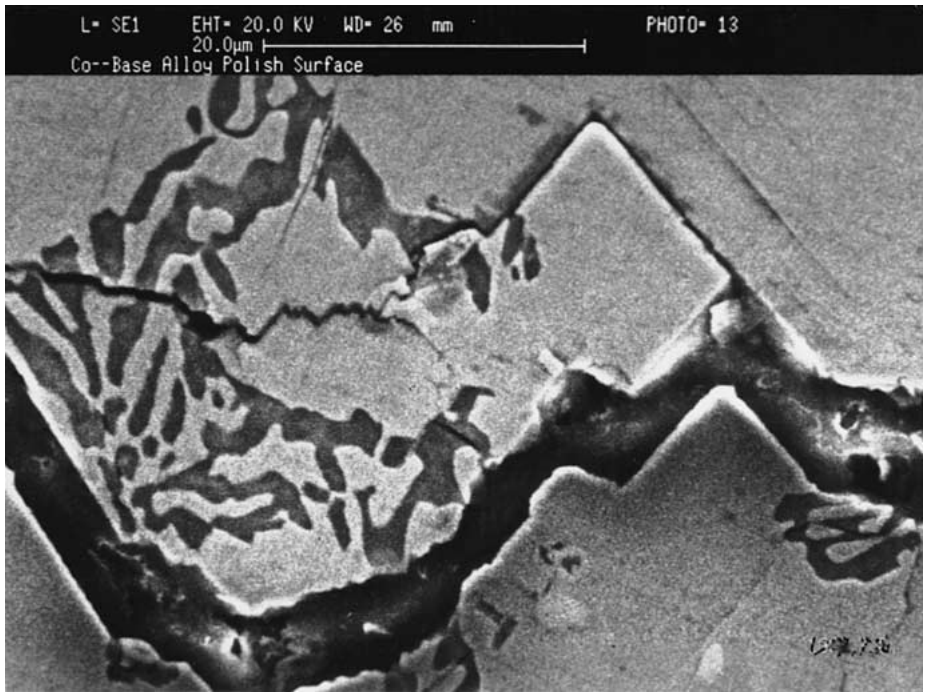

(a)

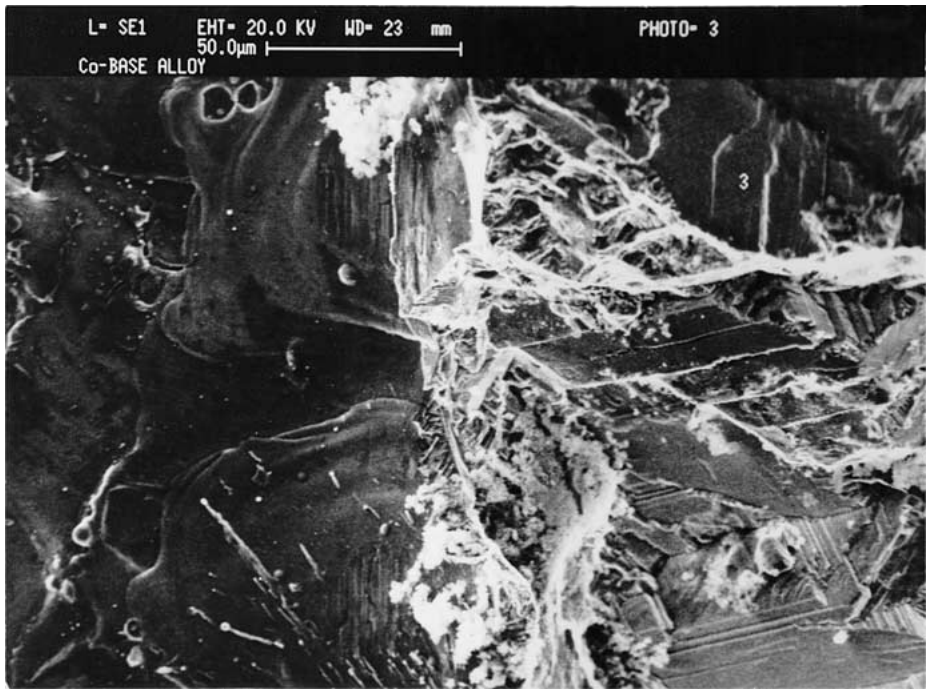

(b)

Figure 5 (a) SEM micrograph showing the crack deflection near the grain boundary. (b) SEM micrograph showing the black debris.

slip bands were observed on the alternating slip planes as shown in Fig. 3c. The slip bands are fine initially and some of the slip bands become coarse with the cycling and shallow cracks initiate at slip band/matrix interface. The size of the fine slip bands is in the range of 600–800 nm and the coarse slip band in the range of 1–2 μm. The threshold intensity for initiating the microcracks in DSX40M alloy for the notched specimen at room temperature is similar to that for the single crystal notched specimen of $Ni_3Al(Cr,B)$ at 400°C under the strain-controlled condition [13]. They observed coarse slip bands with the shallow cracks into these bands. We observe coarse and fine slip bands with shallow cracks. Our results are in good agreement with those of Hsiung *et al*. [15]. They made a successive surface observation on specimen cycled under strain control. At an early stage of cycling they observed that primary slip bands were densely and somewhat uniformly distributed. As cycling proceeds, some of the slip bands become coarser in appearance, and eventually developed into persistent slip bands (PSB) like bands with shallow cracks initiating at PSB/matrix interface.

It can be seen from Fig. 6 that the microcracks initiate at the grain boundaries having carbides/eutectic. Although the grain boundaries are parallel to the loading axis, only a few grain boundaries get severe cracking. The size of the precipitates/carbides was measured with Image Analyzer System. The grain boundaries having

Figure 6 SEM micrograph of the DSX40M alloy surface failed by fatigue showing the microcracks at carbides/eutectic.

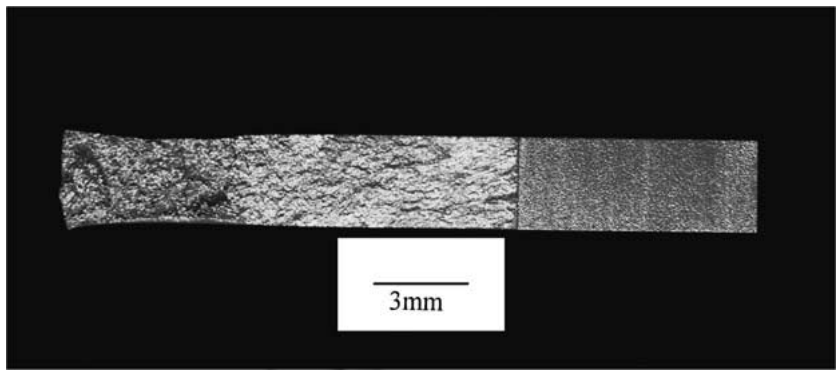

Figure 7 Macroscopic feature of the fractured surface.

carbides/eutectic of size 5 μm or more get severe cracking while the grain boundaries having carbides/eutectic size less than 5 μm do not crack severely. Microcrack starts at the carbide/eutectic and develops in small steps with the fatigue cycles. The slip bands were also observed along the microcracks. It means that the microcracks are under the influence of microstructure as well as under crystallographic slip. At last the developed microcracks join the fatal crack. At the carbides/eutectic stress concentration is high compared to the matrix, so the microcracks start at the carbides/eutectic during the tensile cycling and follow the slip plane. Microcracks were observed at slip bands/matrix interface and these cracks grew with the cycling and join the fatal crack.

Photograph at low magnification shown in Fig. 7 represents two common features (1) the number of microcracks increased with load cycling and (2) the surface length of microcracks increased with increase in number of cycles. Darkness and clarity of the microcracks substantially increased with the increase in fatigue cycles. The observation indicates that the crack opening occurs and hence the crack depth increases. Crack initiated on the surface and propagated into matrix.

SEM micrograph at low ΔK at room temperature is represented in Fig. 8a. The whole view of the fracture surface reveals the typical cleavage fracture and stage I cracking. The octahedral cleavage fracture is shown in Fig. 8b. At room temperature both octahedral and cubic slip in the plastic zone of the coplanar crack tip becomes activated. The cleavage lines in this fracture are at 45° to the loading axis. This indicates that cracking occurs at 45° to the loading directions. The cleavage-like fracture is associated with coplanar slip band cracking. Since the normal stress components associated with a slip band coplanar with a crack depend mostly on the mode I stress intensity factor, the observation that a cleavage-like fracture appearance occurs in DSX40M alloy specimen supports Koss and Chan analysis [7] and the notion that cleavage-like appearance associated with coplanar slip band cracking is the consequence of the crack tip stress field. Fig. 9 represents the ridges on the fracture surface at room temperature. The formation of ridges on the fracture surface is considered to be the result of the following process. Cyclic hardening within primary slip bands ahead of the crack tip leads the secondary slip system into operation

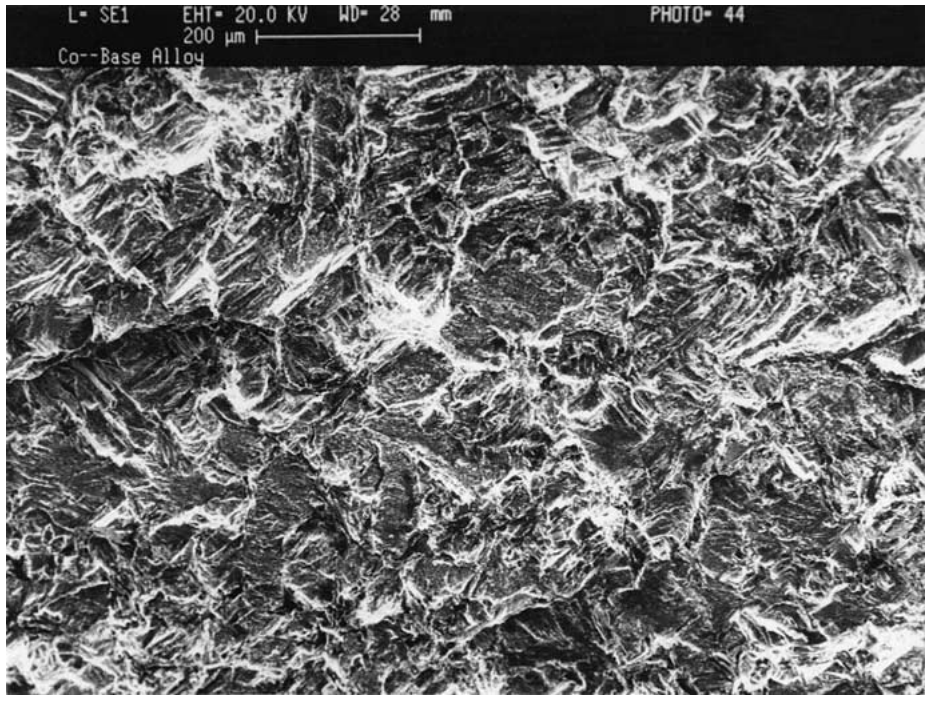

(a)

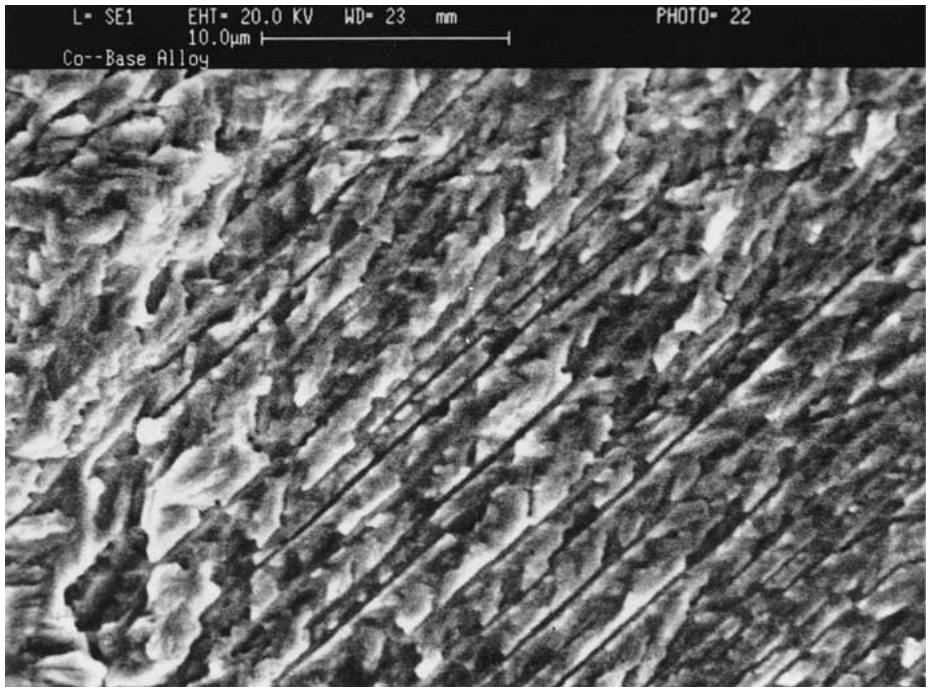

(b)

Figure 8 (a) SEM micrograph at low magnification showing the cleavage fracture. (b) Octahedral cleavage fracture.

and subsequently promotes the crack to propagate onto the secondary slip planes.

Fig. 10 shows the stair-like steps and some pyramids. The formation of the pyramid occurs due to participation of the three planes in the secondary cleavage cracking by intersecting with each other to form pyramid-like features. Such type of features were also observed in a fatigue crack growth of $Ni_3Al(Cr,B)$ single crystal at room temperature [13] and they are arranged approximately normal to the crack propagation. The formation of stair like step occurs due to the participation of two planes in the secondary cleavage cracking by intersecting with each other at right angle to each other. These features are arranged approximately at right angle to crack growth direction. Fatigue striations were also observed as shown in Fig. 11a. Experimental observation of fatigue striations on the fracture surface provides an evidence for the rationale that the fatigue crack growth in DSX40M alloy at room temperature is controlled by multiple slip systems.

Final fracture is the result of tearing that is characterized by dimples on the fracture surface as shown in Fig. 11b. This indicates that the vacancy concentration build up within the fine slip bands by cyclic deformation and prolonged cycling could produce fairly stable vacancy clusters or agglomerates [16] which are

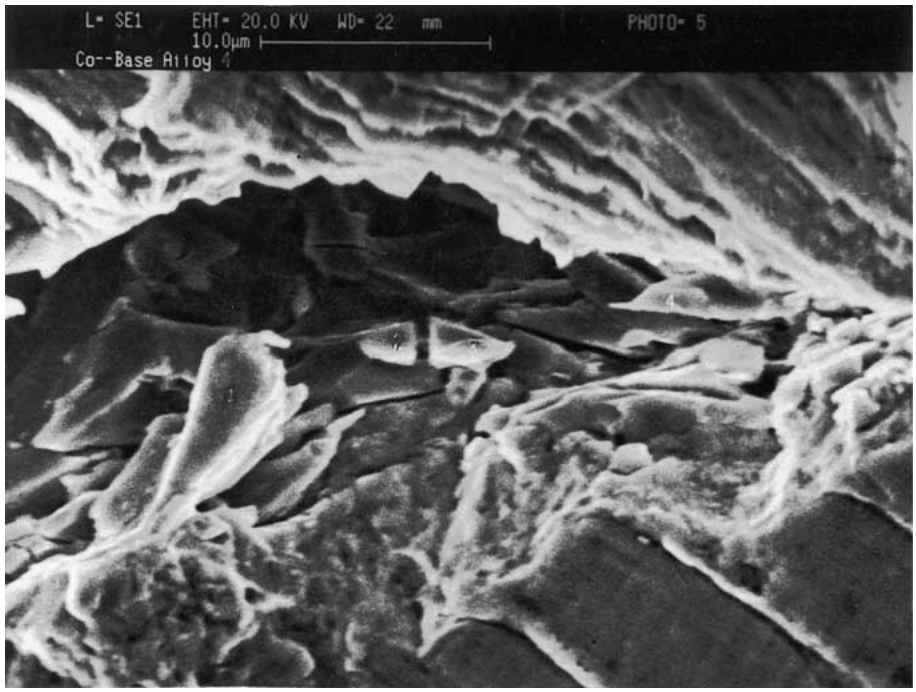

Figure 9 SEM micrographs showing cleavage fracture with ridges on the fracture surface.

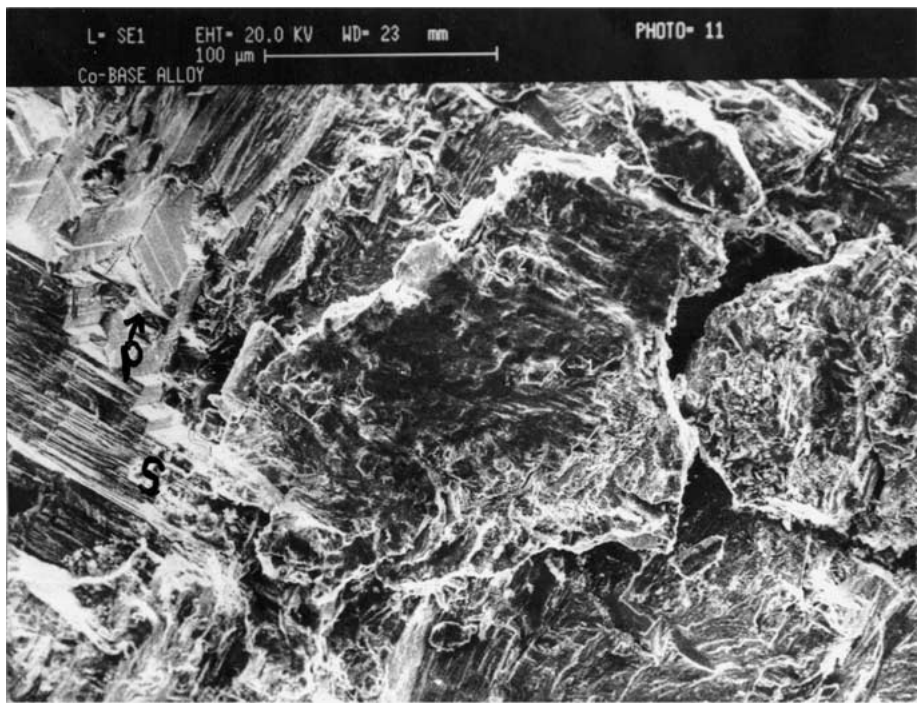

Figure 10 SEM micrograph showing the stair like step (indicated by letter "S") and pyramid like feature (indicated by letter "P").

presumably the preferential sites necessary for absorption of oxygen or water vapour and constitute the void necessary for further development of crack in a local region at the crack tip. As pointed out by Wood [16] vacancy mechanism is most likely brought into effect by fine slip at low stress amplitude. Obviously, the crack growth by vacancy coalescence and absorption of gas is a discontinuous and time dependent process because a certain concentration of vacancies is needed for creating crack nuclei at a given temperature. As some microvoids are observed in the final fracture area so the observed cracking in a DSX40M favours the mechanism proposed by Wood [16]. The build up of edge dislocation dipoles within the slip band enhances the local normal stress across the band and diminishes the surface energy by oxygen absorption and reducing the cohesive strength and promotes local cleavage.

3.3. Crack path and fractographic observation at 850

At 850°C the crack is propagating mainly in mode II. The fractured surfaces were oxidized during the test at 850°C. The cleavage fracture was observed. At

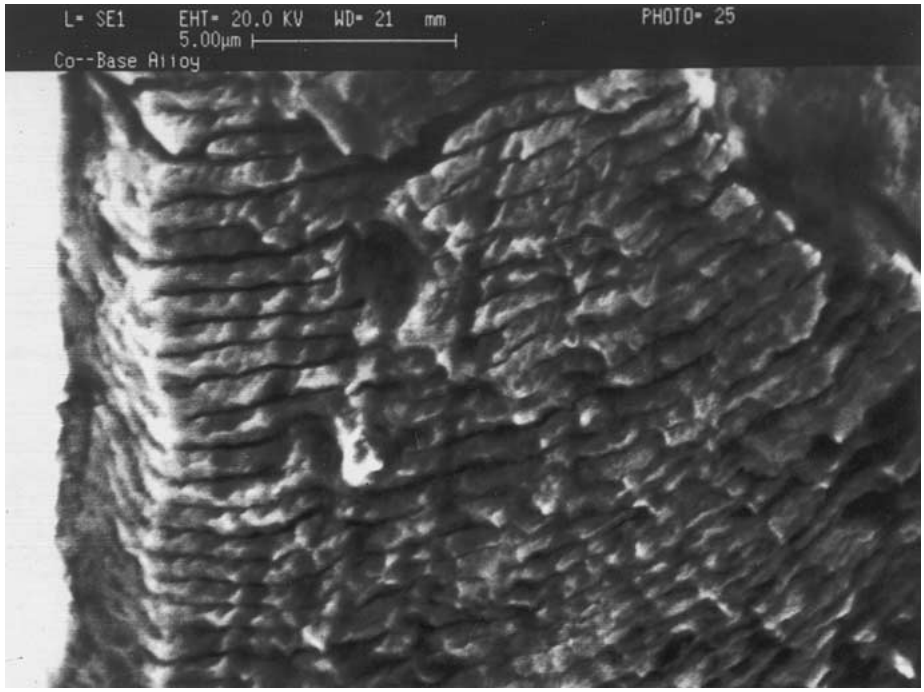

(a)

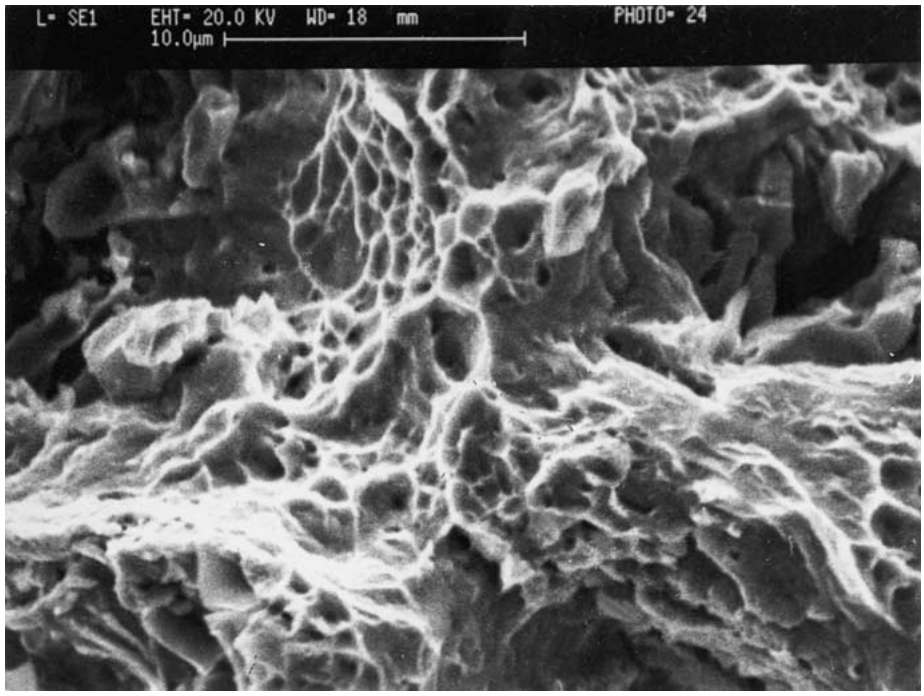

(b)

Figure 11 (a) SEM micrograph showing the fatigue striations at room temperature. (b) Microvoids in the final broken area.

higher ΔK the fatigue striations were also observed. As the surfaces were oxidized, the slip bands were not observed. Microvoids were also observed in the samples and the area of microvoids was large as compared to the samples tested at room temperature. This shows that at higher ΔK the alloy becomes soft at 850°C compared to room temperature.

3.4. Plastic zones dislocation structure at room temperature

Stacking faults and few dislocations were observed in the notch area and is shown in Fig. 12a. The dislocations start moving and piling up in the crack propagation area at lower ΔK as shown in Fig. 12b. The density of the dislocations is very low because the mobility of the dislocations is very slow at room temperature. The transmission electron microscopy clearly revealed the planar slip behaviour of the dislocations as shown in Fig. 12c. The amount of cross slip is reduced because the rearrangement of dislocations is difficult in low energy stacking fault materials.

The density of the dislocations is higher at higher ΔK compared to low ΔK. The micrographs represent dislocations dipoles at higher ΔK as shown in Fig. 12d. Fatigue softening was also observed at RT test. The modification of the dislocations results in the fatigue softening. The network formation of the dislocations

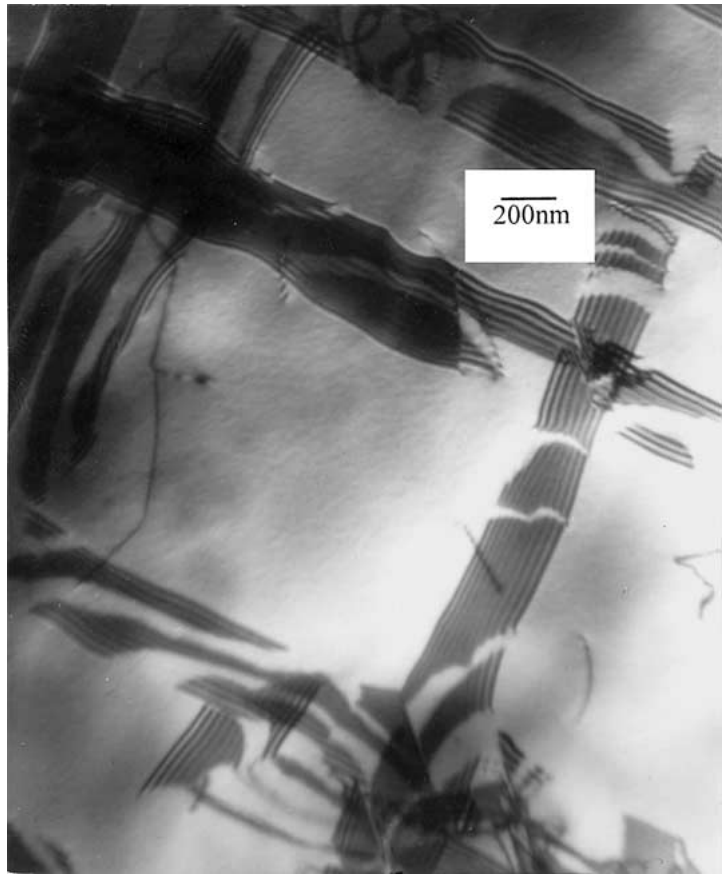

(a)

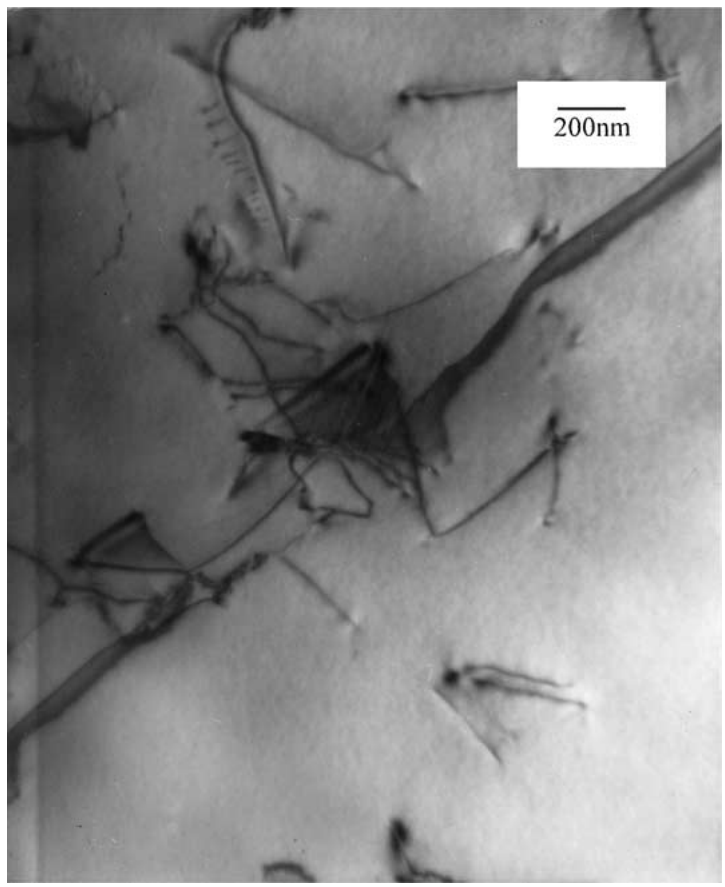

(b)

Figure 12 Transmission electron micrographs represent the (a) stacking faults and dislocation in the notch area. (b) Dislocation pile up in the crack propagation area. (c) The planar slip dislocation. (d) Dislocation dipoles at higher ΔK. (e) The dislocation forming network like structure in the final broken area. (*Continued.*)

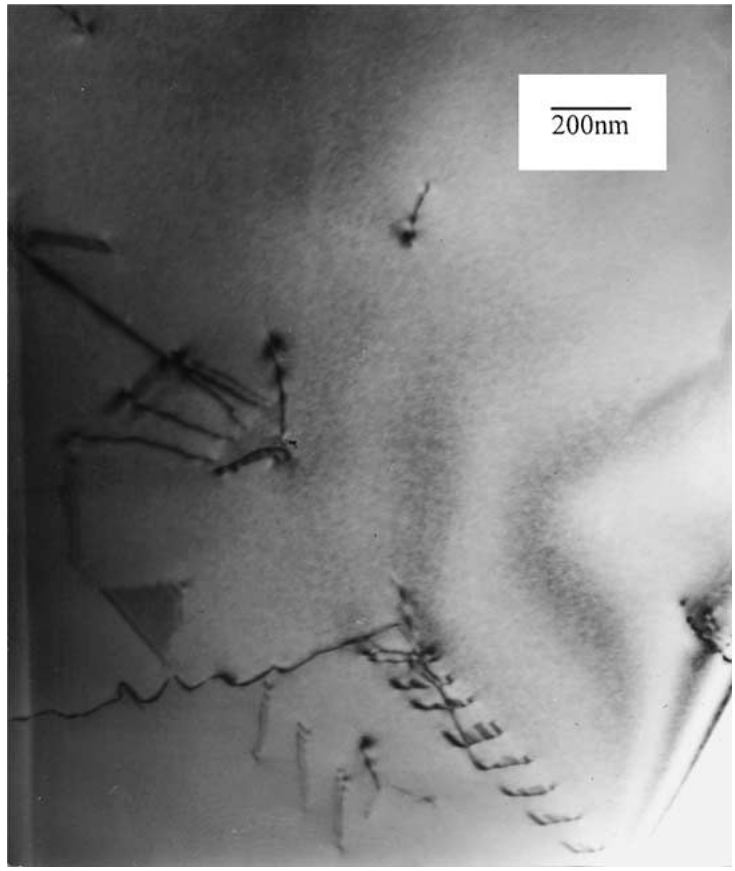

(c)

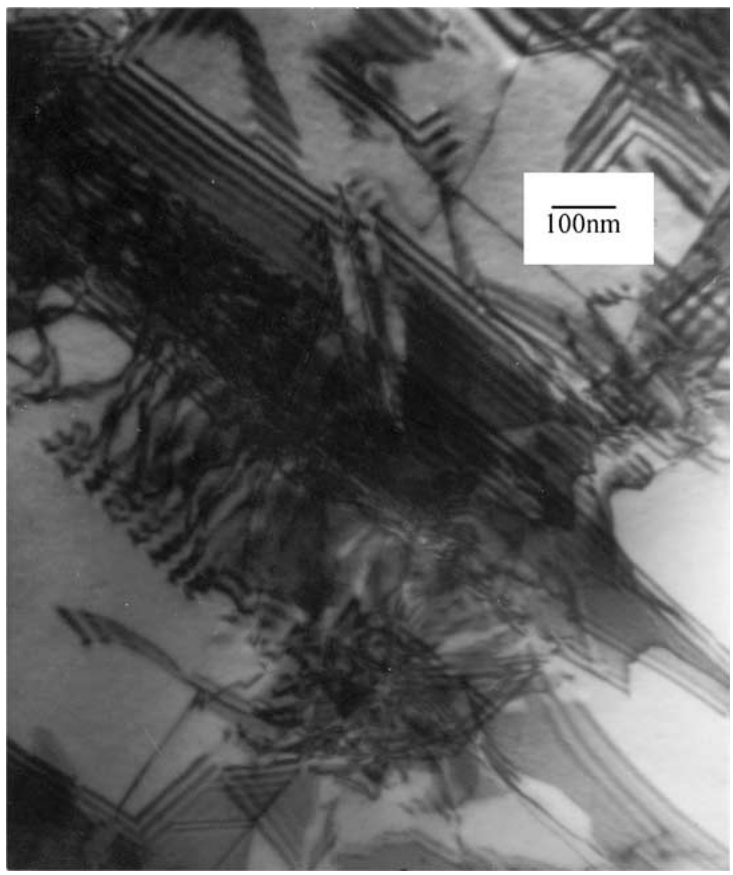

(d)

Figure 12 (*Continued.*)

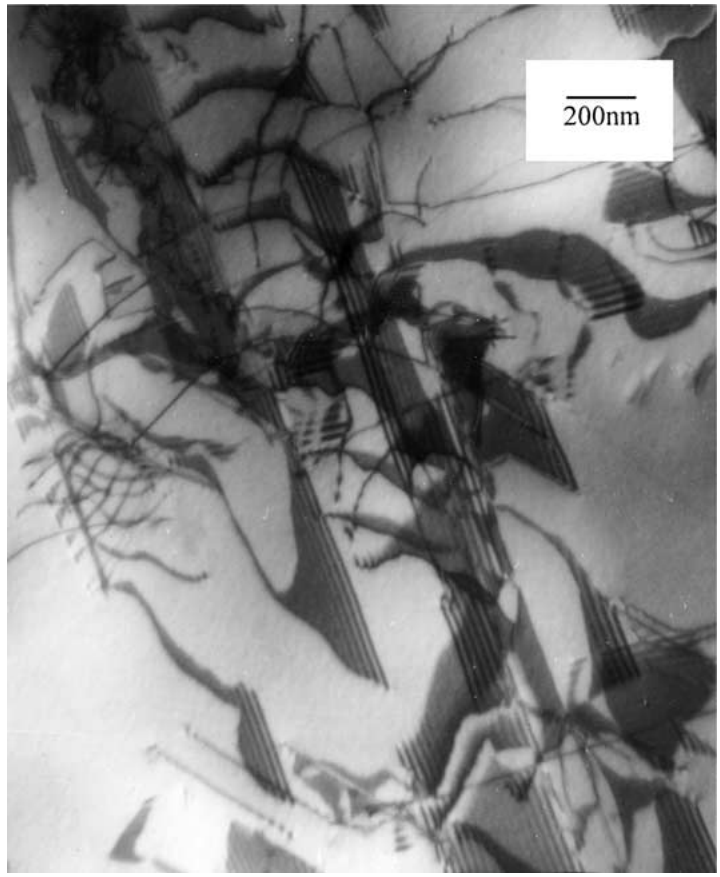

(e)

Figure 12 (*Continued.*)

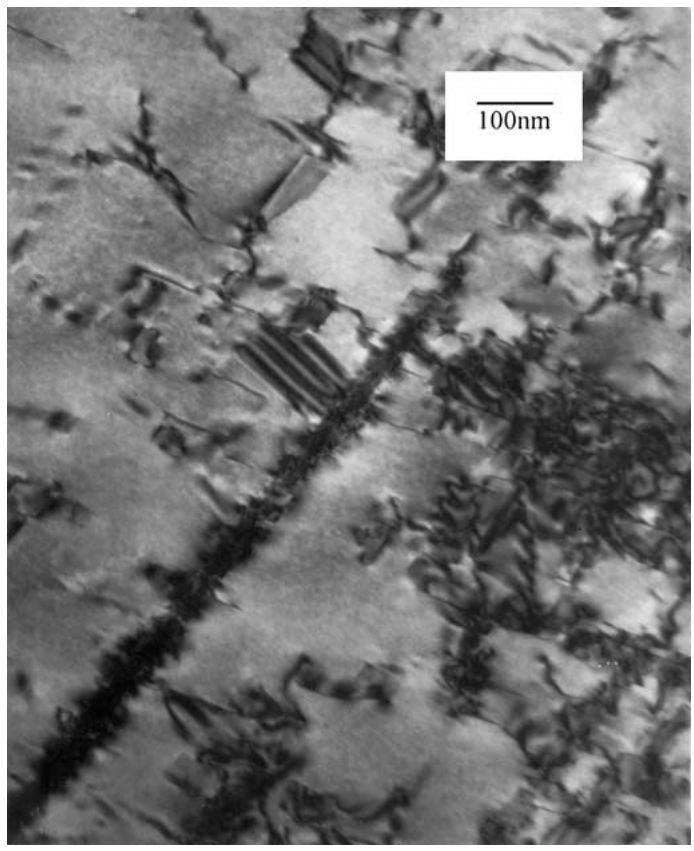

(a)

Figure 13 Transmission electron micrographs show that: (a) dislocations and dislocation dipole pile up in the crack propagation area at low ΔK, (b) dispersing of dislocations and forming a network like structure in the crack propagation area at higher ΔK, (c) dislocations forming a complete network like structure. (*Continued.*)

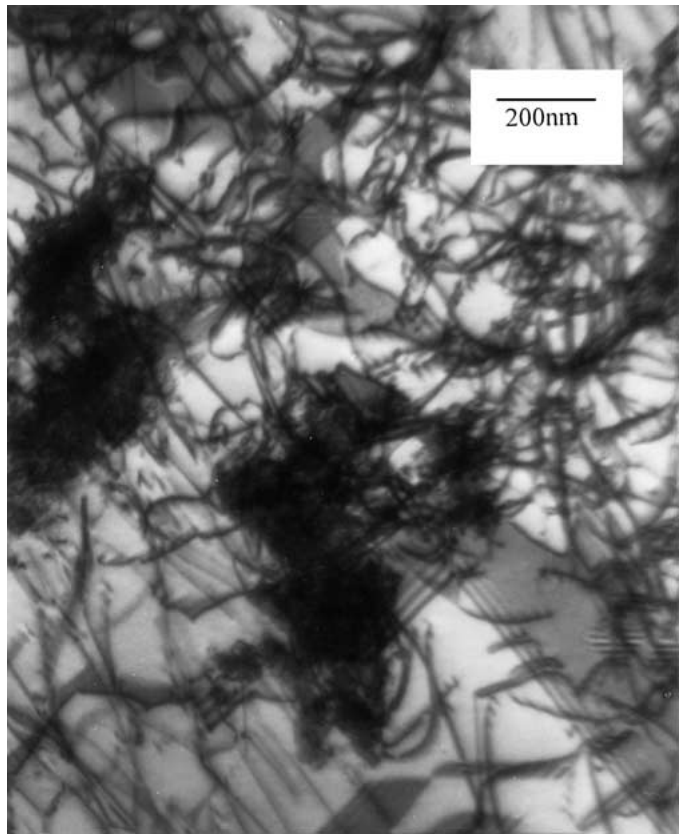

(b)

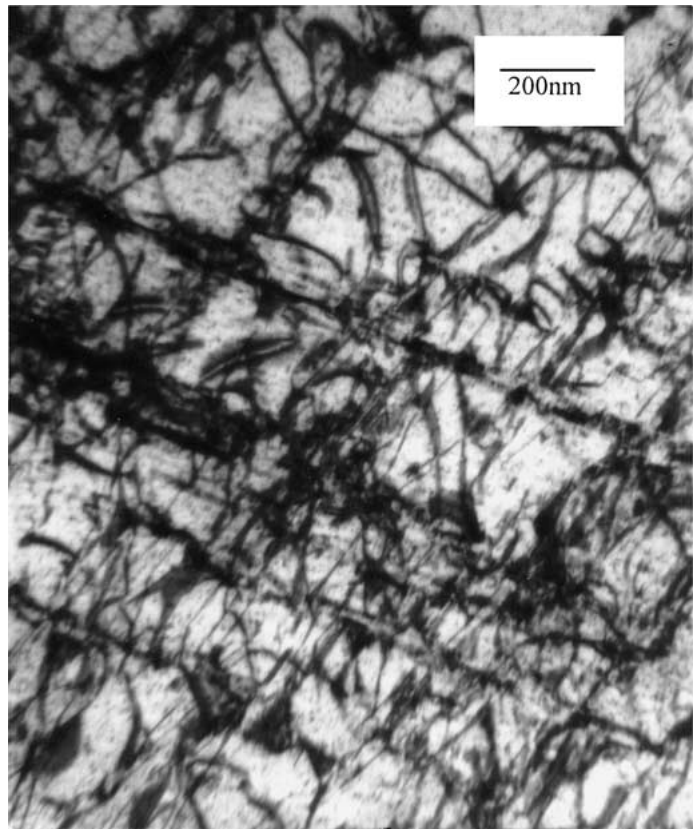

(c)

Figure 13 (*Continued.*)

is observed and is shown in Fig. 12e. This shows that the interaction of dislocations occurs. This modification of the existing dislocation structure taken place in DSX40M alloy at room temperature is the cause of softening at higher ΔK.

3.5. Plastic zone dislocation structure at 850°C

The crack propagation region near the notch represents the dislocation structure and is shown in Fig. 13a. The density of the dislocations is very high and the

dislocations are piling up along the slip band and between the slip bands. The dislocation dipoles are also with these dislocations. The nature of the dislocation is wavy slip. The movement of the dislocations is confirmed underneath the fracture area by the meeting of leading partial and trailing partial at some point as shown in Fig. 13a. At higher ΔK the dislocations are dispersing and trying to form network as shown in Fig. 13b. Very near to final fracture the dislocations are forming a complete network and interacting with the stacking faults as shown in Fig. 13c The dislocation density is very much high compared to room temperature specimens because the mobility of the dislocation is fast at 850°C compared to the room temperature tested samples. In the final fracture area the dislocations form a complete network and leading partial and trailing partial also meet together at some point.

4. Conclusions

The following conclusions can be drawn on the basis of present investigation on the fatigue cracking behaviour of the DSX40M alloy.

(i) Extended stage 1 crystallographic cracking and cleavage fracture occurs in DSX40M alloy under a cyclic tensile load.

(ii) The crystallographic cracking can occur on two or more slip planes simultaneously.

(iii) The number of planes that intersect each other determine the different microscopic features on cleavage fracture surfaces.

(iv) The crack growth rate at 850°C is higher compared to the room temperature in the Paris regime region.

(v) The slip is planar at room temperature and slip is wavy at 850°C.

Acknowledgements

The authors are very thankful to the Third Word Academy of Sciences (TWAS) Italy and Chinese Academy of sciences for providing the financial support for this research work.

References

1. E. CAMPO and V. LUPINIC, *Metall. Sci. and Technol.* **II**(1) (1993) 31.
2. P. E. J. FORSYTH, *Acta Metall.* **11** (1963) 703.
3. M. NAGESWARARAO and V. GEROLD, *Metall. Trans.* **7** (1976) 1847.
4. M. GELL and G. R. LEVERANT, *Acta. Metall.* **16** (1968) 553.
5. D. J. DUQUETTE, M. GELL and J. W. PITEO, *Metall. Trans.* **1** (1970) 3107.
6. C. M. GILMORE, D. E. MCDONALD and W. A. WOOD, *Eng. Fract. Mech.* **5** (1973) 947.
7. D. A. KOSS and K. S. CHAN, *Acta. Metall.* **28** (1980) 1245.
8. H. H. JOHNSON, *Mater. Res. Standard* **5** (1965) 442.
9. K. H. SCHWALBE and D. HELLMANN, *J. Test. Eval.* **9** (1981) 281.
10. Annual Book of ASTM standards, ASTM-E 647, ASTM, Philadelphia, PA, 1984, p. 711.
11. P. NEUMANN, *Acta Metall.* **17** (1969) 1219.
12. P. B. ASWALTH, *Metall. Mater. Trans.* **25A** (1994) 287.
13. G. P. ZHANG, Z. G. WANG, G.Y. LI and S. D. WU, *ibid.* **28A** (1997) 665.
14. R. O. RITCHIE, W. YU, A. F. BLOM and D. K. HOLM, *Fatigue Fract. Eng. Mater. Struct.* **10** (1987) 343.
15. L. M. HSIUNG and N. S. STOLOFF, *Mater. Res. Soc. Symp. Proc.* **133** (1989) 261.
16. W. A. WOOD, *Phil. Mag.* **3** (1958) 692.

Received 29 June 2001
and accepted 30 January 2002